Article:

Design Parameters for Ionic Liquid–Molecular Solvent Blend Electrolytes to Enable Stable Li Metal Cycling Within Li–O₂ Batteries

Alex R. Neale,* Ryan Sharpe, Stephen R. Yeandel, Chih-Han Yen, Konstantin V. Luzyanin, Pooja Goddard, Enrico A. Petrucco, and Laurence J. Hardwick*

Effective utilization of Li-metal electrodes is vital for maximizing the specific energy of lithium–oxygen (Li–O₂) batteries. Many conventional electrolytes that support Li–O₂ cathode processes (e.g., dimethyl sulfoxide, DMSO) are incompatible with Li-metal. Here, a wide range of ternary solutions based on solvent, salt, and ionic liquid (IL) are explored to understand how formulations may be tailored to enhance stability and performance of DMSO at Li-metal electrodes. The optimized formulations therein facilitate stable Li plating/stripping performances, Columbic efficiencies >94%, and improved performance in Li–O₂ full cells. Characterization of Li surfaces reveals the suppression of dendritic deposition and corrosion and the modulation of decomposition reactions at the interface within optimized formulations. These observations are correlated with spectroscopic characterization and simulation of local solvation environments, indicating the persistent importance of DMSO–Li⁺-cation interactions. Therein, stabilization remains dependent on important molar ratios in solution and the 4:1 solvent-salt ratio, corresponding to ideal coordination spheres in these systems, is revealed as critical for these ternary formulations. Importantly, introducing this stable, non-volatile IL has negligible disrupting effects on the critical stabilizing interactions between Li⁺ and DMSO and, thus, may be carefully introduced to tailor other key electrolyte properties for Li–O₂ cells.

1. Introduction

The reliable and widespread application of lithium metal as a highly energy dense anode (11.7 kWh kg⁻¹/3.86 Ah g⁻¹ at

−3.04 V vs the standard hydrogen electrode) in Li-based batteries could represent a significant step change in energy storage capabilities relative to current state-of-the-art Li-ion technologies. Beyond Li-ion, the non-aqueous lithium–oxygen (Li–O₂) battery, generally comprising of a Li-metal anode, a porous cathode framework that accommodates Li₂O₂ growth and an external gaseous O₂ supply as active material, receives particular interest owing to very high specific energies (3500 Wh kg⁻¹ theoretical and 500–1000 Wh kg⁻¹ practical estimates).[1] However, achieving stable cycling of Li-metal anodes, through mitigation of dendritic and decomposition processes, is further complicated in the context of the Li–O₂ battery by the complex processes for the reversible formation/decomposition of Li-oxides at the cathode and the crossover of dissolved gases to the anode (that does not occur in closed systems like Li-ion and Li–sulfur batteries). Understanding these important cathode mechanisms in Li–O₂ cells, and the design of new materials to enable rechargeability at the cathode, is critical to the realization of a practically viable device. Consequently, much of the early Li–O₂ research focused primarily on the cathode interface, and the deleterious processes at the

Dr. A. R. Neale, C.-H. Yen, Prof. L. J. Hardwick
Stephenson Institute for Renewable Energy
Department of Chemistry
University of Liverpool
Liverpool L69 7ZF, UK
E-mail: alex.neale@liverpool.ac.uk; hardwick@liverpool.ac.uk

Dr. R. Sharpe, Dr. S. R. Yeandel, Dr. P. Goddard
Department of Chemistry
Loughborough University
Loughborough LE11 3TU, UK

Dr. S. R. Yeandel
Department of Materials Science and Engineering
University of Sheffield
Sheffield S1 3JD, UK

C.-H. Yen
Department of Chemical Engineering
National Tsing Hua University
Hsinchu 30013, Taiwan

Dr. K. V. Luzyanin
Department of Chemistry
University of Liverpool
Liverpool L69 7ZD, UK

Dr. E. A. Petrucco
Johnson Matthey
Blounts Court Road, Sonning Common, Reading, Berkshire RG4 9NH, UK

Li anode are less considered, or in some cases avoided entirely with the use of unpractical materials as the anode/counter electrode supply of Li^+ (e.g., $Li_{0.5}FePO_4$). The utilization of alternative anode materials has been demonstrated, including high capacity Li–Si alloys and Si-C composites,[2] but these technologies present additional and unique challenges. Therefore, the implementation of Li-metal anodes remains highly desirable to maximize energy densities of Li–O$_2$ cells.

In an ideal Li–O$_2$ full-cell, a chosen liquid electrolyte should exhibit mutual stability at both interfaces, as well as a very low vapor pressure to impede electrolyte evaporation under a dynamic gas supply. However, the high reactivity of both Li-metal and cathode intermediates ensures this is a formidable challenge and many examples that perform well on one side, are unsuitable at the other. The use of solid electrolytes (SE) is an attractive strategy to protect Li-metal due to the perceived safety enhancements over conventional liquid electrolytes.[3] In Li–O$_2$ cells, SEs may eliminate electrolyte loss by evaporation/leakage that is expected in organic molecular solvent-type systems and act as a physical barrier to impede crossover of O$_2$ (and other potential contaminant gases).[4] Furthermore, SEs have enabled the separation of anolyte/catholyte compartments for the use of specifically optimized liquid electrolytes.[5] Despite the improved transport properties in modern SEs, their application remains the subject of extensive research to address key challenges;, for example, stabilization of the Li|SE interface, dendrite formation, interfacial contact resistance, and rate capability.[3,6]

Broadly for non-aqueous liquid electrolytes, additives may be introduced to promote the in situ formation of a solid electrolyte interphase (SEI) layer to impede further electrolyte reduction at Li^0,[7] and to control morphological aspects of Li deposition.[8] Strategies targeting the protection and improvements of Li-metal anodes specifically for Li–O$_2$ battery operation have also been reported in recent years to yield enhancements in cycling stabilities.[9] Notably, pre-treatment methods of the Li electrodes can produce surface films that modulate plating mechanisms (inhibiting dendritic deposition/stripping) and impede decomposition pathways in electrolytes suitable for Li–O$_2$ cathodes. For example, direct reaction of molten Li with poly(tetrafluoroethylene) particles (under Ar) was shown to produce a beneficial surface layer consisting of a gradient of LiF and F-doped carbon phases.[9d] Therein, the surface film on pre-treated anodes promoted uniform deposition of Li^+, mitigating dendrite formation, and reduced corrosion reactions, translating directly to more than double the cycle lifetime to 180 cycles versus 78 cycles in control Li–O$_2$ full cells with untreated Li anodes.

In recent years, groups have reported positively on the use of highly concentrated electrolytes (HCEs) with enhanced cyclability at Li-metal and Columbic efficiencies upward of 99%, with many examples using lithium bis(fluorosulfonyl) imide (Li[FSI]) in ether or carbonate solvents.[10] The new concept of localized high concentration electrolytes (LHCEs) is also a valuable strategy, where a non-solvating inert diluent (e.g., fluorinated ethers) is introduced to promote transport properties (and reduce salt costs) while retaining the key local Li^+-solvation interactions of a highly concentrated system. However, the instability toward oxygen reduction of carbonate solvents,[11] and the $[FSI]^-$ anion,[12] as well as the significant volatility of both the frequently used low boiling ethers (frequently used in HCEs, for example, 1,2-dimethoxyethane) and the fluorinated ethers (used to form LHCEs) indicates these routes may not be applicable for practical Li–O$_2$ cells.

Unlike these components, dimethyl sulfoxide (DMSO) is generally considered an advantageous solvent at the Li–O$_2$ cathode, owing to moderate vapor pressures and the high donor number mediation of large discharge capacities.[13] However, in addition to some side reactions at the cathode,[14] DMSO rapidly undergoes severe decomposition reactions with Li^0. In this regard, there has been work in recent years demonstrating the enhancement in stability for DMSO by the use of additives,[15] and the formulation of HCEs.[16] A recent proof-of-concept investigation also demonstrated the use of a liquid/liquid interface with a secondary non-soluble electrolyte to enhance stability by blocking direct DMSO-Li^0 interaction.[17] Similarly, the performance of *N,N*-dimethylacetamide, a solvent with comparable reactivity at Li^0, was shown to be improved in Li–O$_2$ full cells with careful optimization of the salt composition at high concentrations to regulate the formation of a beneficial SEI.[18]

Ionic liquids (ILs) are another candidate solvent class owing to their potential for great (electro)chemical and thermal stabilities, as well as negligible vapor pressures that would mitigate evaporation issues in Li–O$_2$ cells. ILs can facilitate low charging overpotentials in the absence of redox mediators,[19] and recent work has demonstrated the functionalization of an IL with redox mediator groups that provided a component structure that supports rechargeability and anode stability.[20] However, the utilization of ILs is plagued by sluggish transport properties that can limit meaningful rate capabilities at room temperature. Considering also the established stability and volatility challenges of conventional molecular solvents, the formulation of blended IL/molecular solvent formulations have been shown as an important strategy to manipulate electrolyte properties for battery and supercapacitor applications,[21] including the blending of DMSO with ILs for Li–O$_2$ studies.[22]

In this work, a comprehensive experimental and computational approach toward understanding formulation design of molecular solvent/IL/salt ternary blend electrolytes for Li–O$_2$ cells is detailed. By tailoring the ratios of readily available, Li–O$_2$ cathode-relevant materials, DMSO, 1-butyl-1-methylpyrrolidinium bis{(trifluoromethyl)sulfonyl}imide ([Pyrr$_{14}$][TFSI]), and Li[TFSI] salt, a wide formulation range is explored to systematically target and understand desired synergistic properties relating to Li-anode stabilities. Encompassing some parallels with HCEs/LHCEs, Li metal electroplating/stripping with high Columbic efficiency is achieved in the presence of reactive DMSO in the ternary formulations, and operation at both anode and cathode interfaces of Li–O$_2$ cells is improved. Spectroscopic and computational characterization, in conjunction with electrochemical and surface characterization measurements, is used to understand requisite properties and, critically, the solvation environments in the presence of the IL that permit the observed stabilization effects in these ternary formulations.

2. Results and Discussion

2.1. Electrochemistry of Li Plating and Stripping

The reactivity, or instability, of DMSO in conventional electrolyte formulations toward Li metal (in the absence of strong SEI forming additives) is first demonstrated using symmetrical Li|electrolyte|Li coin cells under galvanostatic control (**Figure 1** (i)). Therein, plating/stripping potentials of a simple binary electrolyte of 0.7 mol dm^{-3} Li[TFSI] in DMSO experience dramatic fluctuations, rising steeply from the first few cycles. This is attributed to direct and continuous decomposition reactions of DMSO at the Li-metal interface. By contrast, through simple addition of [Pyrr$_{14}$][TFSI] IL in to the solution of Li[TFSI] in DMSO, the apparent stability of the electrolyte toward lithium metal is enhanced significantly with limited change in plating/stripping overpotentials (η) for over 400 h of cycling. [Pyrr$_{14}$][TFSI] was selected as the IL component, with reliable commercial availability at high purities (to investigate a facile strategy using readily available materials), owing to its established

excellent electrochemical stability (>5.8 V stability window),[23] good oxygen electrochemistry,[24] and good performance in full Li–O$_2$ cells.[19a] The reasonable stability of quaternary ammonium-[TFSI] ILs like [Pyrr$_{14}$][TFSI] toward Li plating/stripping has been demonstrated previously.[12,25] However, the ternary mixture presented nevertheless contains ≈50 mol% of the more reactive DMSO.

To study the origins of Li anode stabilization and improved performance of the blended electrolytes, binary and ternary formulations of DMSO, Li[TFSI], and [Pyrr$_{14}$][TFSI] were prepared across a range of known molar fractions (and molar ratios) based on the ternary plot in Figure 1 (ii). Therein, mixtures were prepared with fixed ratios between the DMSO and IL components (x_{DMSO}:$x_{[Pyrr14][TFSI]}$) and these mixtures are respectively grouped by straight lines in Figure 1 (ii) and labeled solutions A(1:0), B(9:1), C(8:2), and D(6:4). The final numerical molar fractions of the prepared ternary formulations containing Li-salt, as well as important molar ratios and molalities, are provided in Table S1, Supporting Information. Samples containing high molar fractions of Li-salt required
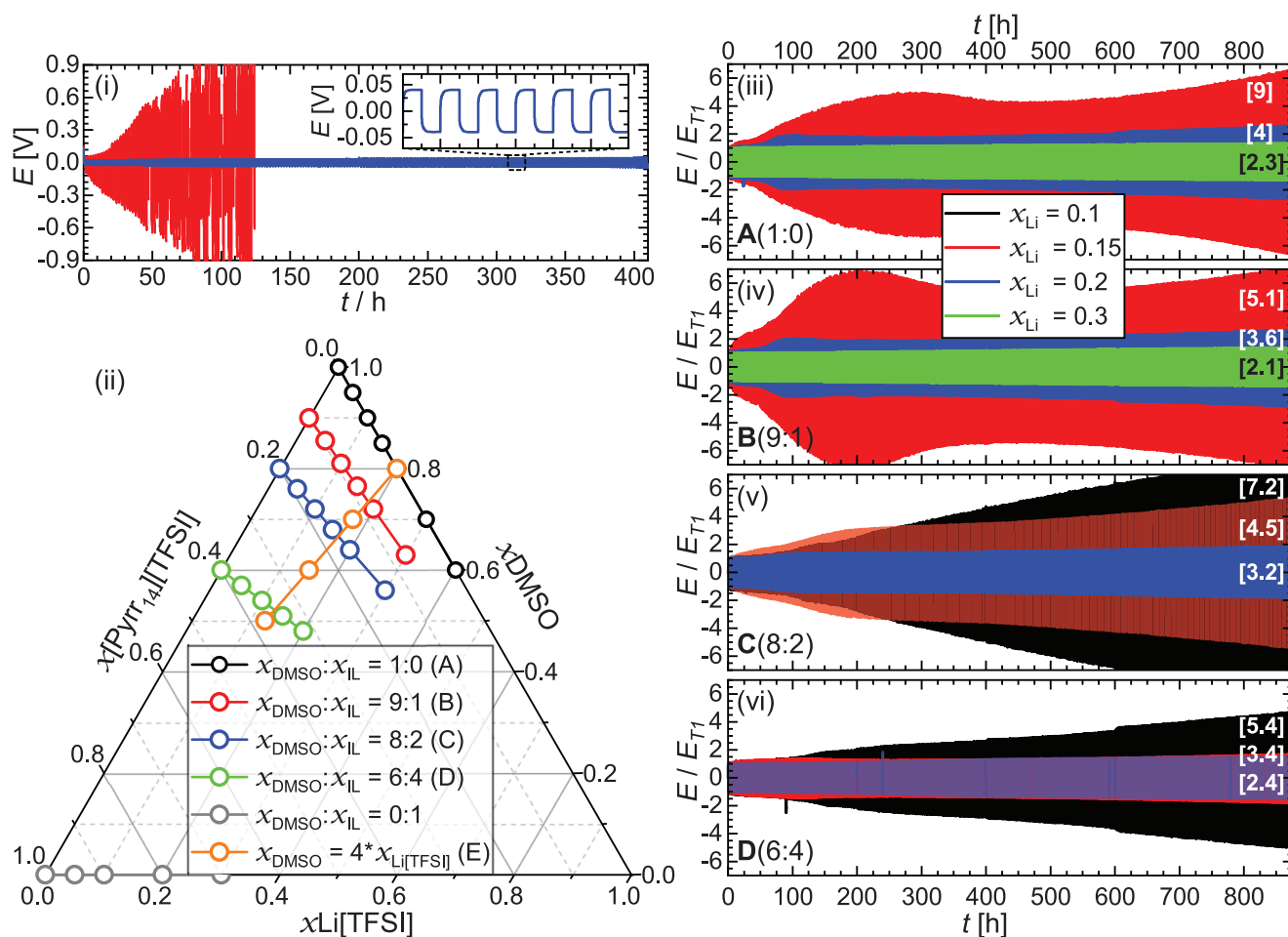
Figure 1. i) Galvanostatic cycling of Li|electrolyte|Li coin cells containing 0.7 mol dm^{-3} Li[TFSI] in DMSO (red trace) and in (0.6)DMSO–(0.4)[Pyrr$_{14}$][TFSI] (blue trace). Inset zooms in on stable appearance of plating stripping in IL/solvent/Li-salt ternary mixture. ii) Ternary plot showing the formulations of DMSO, Li[TFSI], and [Pyrr$_{14}$][TFSI] studied in this work. iii–vi) Normalized voltage (E/E_{T1}) profiles of Li|electrolyte|Li symmetrical cells for the A(1:0), B(9:1), C(6:4), and D(6:4) binary/ternary solutions, respectively. Bracketed numbers highlight the molar ratio of DMSO to Li$^+$ in each solution. Cells were cycled at $j = \pm 0.05$ mA cm^{-2} for 1 h per half-cycle ($Q = 0.05$ mAh cm^{-2} per half-cycle).

**ADVANCED
SCIENCE NEWS**
www.advancedsciencenews.com

**ADVANCED
FUNCTIONAL
MATERIALS**
www.afm-journal.de

gentle heating to form homogenous solutions where the majority of prepared formulations remained liquid once cooled to room temperature. The melting point for the solution containing $x_{Li} = 0.4$ in DMSO [A(1:0)] was approximately room temperature and, consequently, this sample was not used for electrochemical measurements. Formulation D(6:4) containing $x_{Li} = 0.3$ was also prepared with gentle heating, but precipitated out of solution when cooled down to room temperature.

The stability of the prepared formulations toward Li metal cycling was screened through successive plating/stripping cycling in symmetrical Li|Li cells. Therein, any increase in measured η of the plating/stripping processes is indicative of continued interfacial decomposition reactions. Conversely, minimal changes in η, in the absence of a strong SEI forming component (relative to established SEI-forming components like vinylene carbonate or fluoroethylene carbonate),[26] are ascribed to improved resilience of the electrolyte toward reductive decomposition at the Li anode. Given the inevitable lower fluidity (i.e., higher viscosity and poorer ionic mobility) of formulations containing large fractions of Li[TFSI] and [Pyrr$_{14}$][TFSI], higher values of η for plating/stripping are expected relative to the more conductive DMSO-rich solutions. Consequently, for better comparison of relative stability changes, the cycling voltages (E) are normalized versus the terminal voltage (E_{T1}) of the first plating step. The normalized voltage (E/E_{T1}) profiles over 900 h of cycling are presented in Figure 1 (iii–vi). The absolute, non-normalized, cycling data and the expanded voltage profiles at select cycling times are presented in Figures S1 and S2, Supporting Information, respectively. Given the instability of $x_{Li} = 0.1$ in solutions A(1:0) and B(9:1) on these timescales (where $E/E_{T1} > 10$ at ≈200 h), these data are excluded from Figure 1 (iii–vi) for clarity and provided only in Figure S1, Supporting Information.

In brief, the cycling performance of DMSO rich (IL- and Li-poor) formulations is unsurprisingly poor owing to the established high reactivity of DMSO solvent toward Li^0. Conversely, solutions with greater IL and Li-salt fractions remain more stable and exhibit minimal changes in observed cycling potentials. By formulation of IL- and Li[TFSI]-rich electrolytes, stable Li plating/stripping cycling (i.e., where η remains consistent) can be achieved for over 800 h. Critically however, for all solutions where E/E_{T1} remains less than ≈2 after 800 h (400 cycles), it is found that the ratio of $x_{DMSO}:x_{Li[TFSI]}$ is less than 4:1 (as highlighted by square bracketed values in Figure 1 (iii–vi). Despite some of the more IL-rich solutions containing significantly reduced molar quantities of the reactive DMSO (e.g., $x_{Li} = 0.1$ in C(8:2) and D(6:4) where $x_{DMSO} = 0.72$ and 0.54, respectively), stable cycling of Li is not achieved. The general trends observed in symmetrical Li|Li cells in Figure 1 (iii–vi) and Figure S1, Supporting Information initially point toward the distinctive importance of the DMSO:Li$^+$ interactions even in the more complex ternary mixtures.

The evolution of impedance in Li|Li cells was investigated by electrochemical impedance spectroscopy (EIS) in a selection of electrolyte formulations ($x_{Li} = 0.1$ in A(1:0); 0.2 in A(1:0); 0.2 in C(8:2)). The resulting Nyquist plots, collected at open circuit potential at 50 cycle intervals, are presented in **Figure 2** (i-iii) and the overpotential profiles for the studied cells are shown in Figure 2 (iv). Therein, the Nyquist plots consist of

a high-to-mid frequency depressed semicircle, attributed to interfacial/SEI resistance, and a mid-to-low frequency response (≈<50–100 Hz) originating from charge transfer resistance contributions.[27] The evolution in interfacial resistance (R_{int}) and charge transfer resistance (R_{ct}) in the studied cells is presented in Figure 2 (v,vi), respectively, estimated from fitting the impedance response to the equivalent circuit shown in Figure 2 (vi). Within the less concentrated binary electrolyte ($x_{Li} = 0.1$ in A(1:0), Figure 2 (i), the magnitude of both impedance contributions increases continually up to 200 cycles and the high-frequency intercept (originating from bulk electrolyte resistance, R_{bulk}) increases by 235% from 3.4 to 11.4 Ω. In accordance with the increasing plating/stripping overpotential in this cell, these changes indicate the continual consumption of electrolyte by decomposition reactions and the growth of a thicker, less stable passivating surface film. It is noteworthy that this formulation, while more dilute than the comparisons here, still contains a reasonable molal concentration of 1.4 mol kg^{-1}. For both the more concentrated binary (Figure 2 (ii)) and ternary (Figure 2 (iii)) electrolytes, the initial enhancements in impedance seen after the first 50–100 cycles appear to stabilize or reduce with progressive cycling (while R_{bulk} increases by only 37% and 20% over 200 cycles for 0.2 in A(1:0) and 0.2 in C(8:2), respectively). This initial growth of R_{int} in the first interval after cycling indicates changes in the Li/electrolyte interface, presumably related to growth and evolution of a more reliable Li$^+$-conducting SEI (discussed later). However, R_{ct} is consistently larger for the ternary formulation and can be associated in part to the poorer fluidity compared to the binary solution,[28] possibly exacerbated by morphological changes of the Li surface.

Scanning electron microscopy (SEM) images of Li electrode surfaces taken from analogous Li|Li cells after 100 plating stripping/cycles are provided in Figure S3, Supporting Information. Within the less stable binary solution ($x_{Li} = 0.1$ in A(1:0), Figure S3 (i,ii), Supporting Information), the Li electrode shows clear surface microstructures relating to pitting reactions and dendritic deposition, and large fractures in the bulk surface caused by significant corrosion. The more concentrated binary and ternary formulations, however, appear to facilitate more stable, uniform plating/stripping processes with comparatively minimal surface features present after 100 cycles and much less evidence of corrosion or fractures in the anode surface (Figure S3 (iii–iv), Supporting Information). The suppression of dendritic deposition of Li in high concentration electrolytes, and their stabilizing effects on the SEI, has been demonstrated and investigated previously.[29] Additionally, dendrite-suppressed plating/stripping of Li has also been achieved with the use of ILs as electrolyte solvents or co-solvents.[25b,30] Notably, synergy between IL and Li salt concentrations in ether-based, Li–S battery electrolytes was found to stabilize the resulting SEI and suppress dendritic deposition in parallel.[31] Achieving uniform Li plating without dendrite formation is critical to functioning Li metal electrodes not only due to safety concerns associated with short circuiting cells, but also to impede the continual decomposition reactions on fresh Li dendrite surfaces and the loss of electrically disconnected, inaccessible Li as "dead lithium."

While the symmetrical Li|Li cell data present a valuable comparison between behaviors of different electrolytes at the Li-metal electrode, the absolute utilization of the available Li
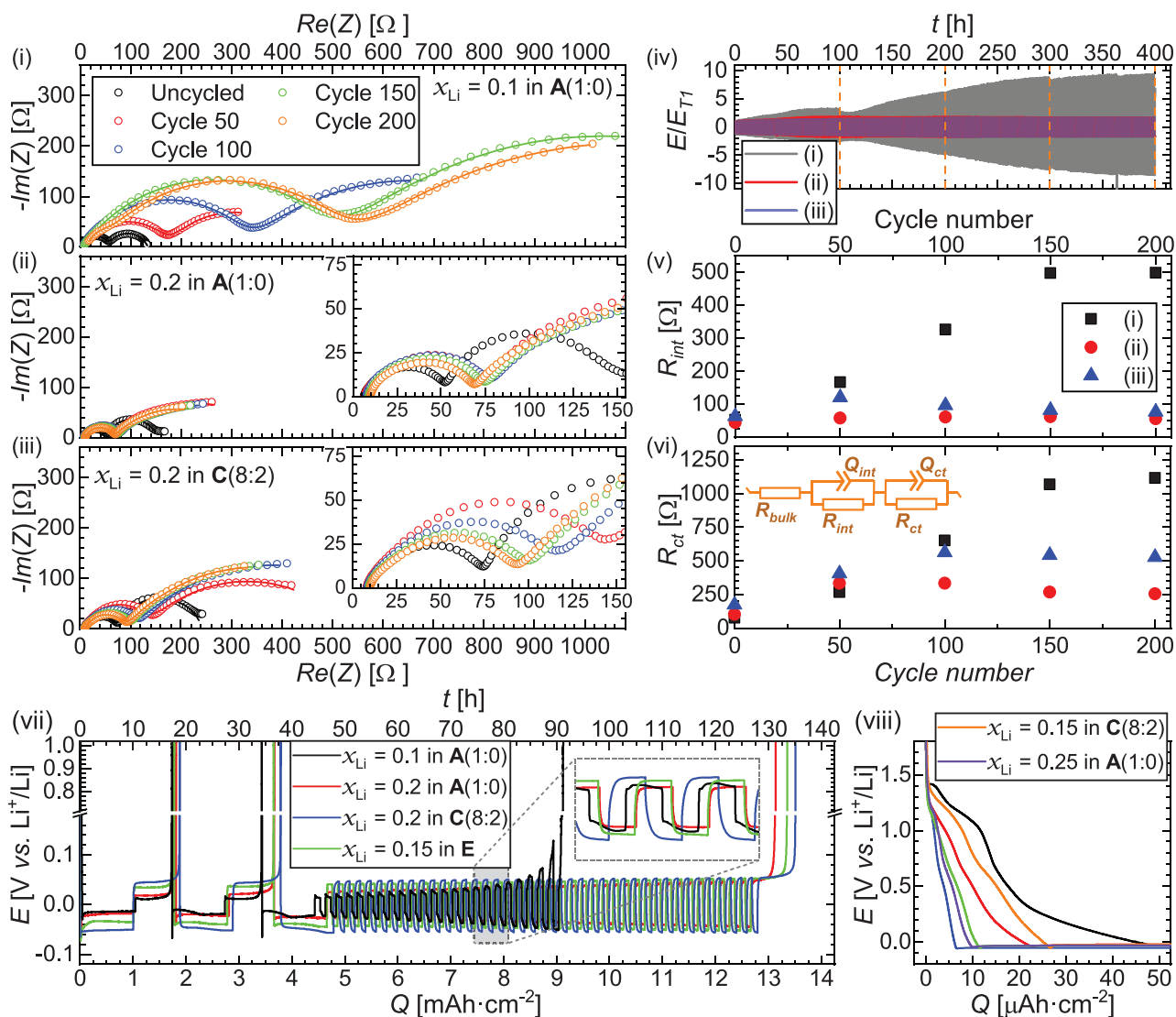
Figure 2. i–iii) Nyquist plots of Li|Li symmetrical cells at 50 cycle (100 h) intervals for electrolytes $0.1x_{Li}$ in A(1:0) (i), $0.2x_{Li}$ in A(1:0) (ii), and $0.2x_{Li}$ in C(8:2) (iii). Solid lines represent the simulated EIS data and the inset data highlights the changes in the high frequency region. iv) Voltage profiles, cycled at $j = \pm0.05$ mA cm^{-2} for 1 h per half-cycle, for cells shown in the Nyquist plots. v) Interfacial resistance (R_{int}) and vi) charge transfer resistance (R_{ct}) extracted from impedance data simulation of (i–iii) based on the pictured equivalent circuit. vii) Example voltage profiles for Columbic efficiency measurements in Li|Cu cells. Inset data highlights some differences in voltage profiles during the short cycling step. viii) Initial pre-plating reducing capacity during the first plating step in Li|Cu cells. The additional traces in (viii) correspond to the legend colors in (vii). The Li|Cu cells were cycled at $j = \pm0.1$ mA cm^{-2} and full description of the current/capacity regime is provided in the Experimental Section, Supporting Information.

metal is very low (<0.1% per half-cycle) due to the relative thickness of the Li foil used herein. Indeed, under a slightly higher capacity (and current density) regime, the electrolytes do follow similar trends in stability in Li|Li cells as presented in Figure S4, Supporting Information, wherein the formulations rich in both IL and Li-salt are able to cycle for the longest time without failure. However, as has been described in recent years, to reach practically viable energy densities within Li-metal cells, Li utilization should be approaching or exceeding 80% per cycle and, if possible, suitably thin foils should be utilized.[32] To replicate more realistic scenarios, and to further understand electrolyte stability at freshly deposited/stripped Li^0 surfaces, the Columbic efficiency (CE) of the plating/stripping process was

measured using asymmetric Li|Cu cells according to similar testing regimes described by Adams et al. (see Experimental Section, Supporting Information for full details).[33] Following 2 initial conditioning steps to negate substrate effects, a Li reservoir (of capacity Q_T) is deposited on the Cu electrode and then stripped/plated through $n = 40$ successive cycles (of capacity Q_c) and, finally, exhaustively stripped to a 1.2 V versus Li$^+$/Li limit to give the final stripping capacity, Q_s. The average CE can then be derived from Equation 1:

$$CE = \frac{(nQ_c + Q_s)}{(nQ_c + Q_T)} \times 100 \quad (1)$$

**ADVANCED
SCIENCE NEWS**

www.advancedsciencenews.com

**ADVANCED
FUNCTIONAL
MATERIALS**

www.afm-journal.de

Table 1. Average Columbic efficiency (*CE*) for select binary/ternary formulations, the efficiency of the first two conditioning steps (E_1 and E_2), and the initial pre-plating capacity (Q_{init}) during the first application of reducing current in Li|Cu cells. Error values derived from the standard error of multiple repeat cells.

Sample	x_{DMSO}/x_{Li}	CE [%]	E_1 [%]	E_2 [%]	Q_{init} [μAh cm^{-2}]
$0.1x_{Li}$ in A(1:0)	9	71.7	69.3	69.5	45.0
$0.2x_{Li}$ in A(1:0)	4	88.6 ± 0.8	77.4 ± 2.1	83.6 ± 1.5	20.7
$0.25x_{Li}$ in A(1:0)	3	93.4 ± 0.1	87.1 ± 0.5	89.9 ± 0.4	9.2
$0.15x_{Li}$ in C(8:2)	4.5	89.8 ± 1.2	75.4 ± 1.1	85.1 ± 1.2	25.2
$0.2x_{Li}$ in C(8:2)	3.2	94.3 ± 0.1	87.9 ± 0.1	89.6 ± 0.8	6.1
$0.15x_{Li}$ in E	4	92.5 ± 0.5	75.5 ± 0.8	88.4 ± 0.6	10.7

Some example voltage profiles of Li|Cu cells with select electrolyte formulations are shown in Figure 2 (vii). The calculated Columbic efficiencies and the associated standard error from the spread between measurements that did not fail are detailed in **Table 1**. The efficiency of the first two conditioning steps is also presented. Congruent with earlier results, the more dilute solution (x_{Li} = 0.1 in A(1:0), black trace) containing no IL component displayed unstable voltage profiles due to the reactivity of DMSO and, consequently, failed before reaching the final stripping step (approximating to *CE* ≈ 71%). This behavior was reproduced in numerous Li|Cu cells. By increasing salt concentration in the binary DMSO:Li[TFSI] mixtures to give the molar ratio of 4:1 (i.e., x_{Li} = 0.2 in A(1:0), red trace), more stable voltage profiles are observed and, importantly, the derived *CE* is enhanced to 88.4%. Likewise, further increasing salt concentration in DMSO to a ratio of 3:1 (DMSO:Li[TFSI], that is, x_{Li} = 0.25 in A(1:0)) resulted in further efficiency improvements, yielding 93% *CE* under these test conditions. Concerning the ternary solutions, good stability enhancements relative to more dilute or IL-free solutions is achieved by moderate introduction of IL to the electrolyte (x_{Li} = 0.15 in C(8:2)), increasing *CE* to 89.6% despite the ratio of $x_{DMSO}:x_{Li+}$ exceeding 4:1. However, when both Li-salt and IL concentrations are increased such that $x_{DMSO}:x_{Li+}$ is reduced below 4:1, the ternary formulation (x_{Li} = 0.2 in C(8:2) presents the best *CE* (>94%) among the materials studied in this work.

To further understand the effect of the IL on these systems, electrolytes were designed with varying IL proportions where $x_{DMSO}:x_{Li[TFSI]}$ is fixed at 4:1 (labeled as solution E, green trace in Figure 2 represented by the orange points in Figure 1 (ii) and detailed in Table S1, Supporting Information). When compared to the binary mixture of the same ratio (i.e., x_{Li} = 0.2 in A(1:0), red trace), the resulting stability enhancement yielded less growth in η with cycling and an improved *CE* of 92.4%. Nevertheless, while the IL component surely contributes somewhat to the improved interfacial stabilities with Li-metal, the combination of a higher IL content with low DMSO:Li ratios also results in the largest overpotentials in all cases.

The poor Columbic efficiency of low-to-moderately concentrated DMSO/Li[TFSI] electrolytes is expected and has been reported previously (1 mol dm^{-3} Li[TFSI] in DMSO, *CE* ≈ 25–50%).[15,16c,34] Additionally, the stability enhancements gained from more highly concentrated DMSO/Li[TFSI] have

been reported in symmetrical Li|Li cell cycling and by observation of Li-metal surfaces by SEM,[16a] as well as a Columbic efficiency of ≈85% in 3 mol dm^{-3} Li[TFSI] in DMSO.[16c] However, the apparent stabilization realized in the IL-containing solutions, $0.2x_{Li}$ in C(8:2) and $0.15x_{Li}$ in E, are found to be larger. These values even exceed that achieved by introduction of two well-established SEI forming components, vinylene carbonate and Li[NO$_3$],[15] and is comparable to highly concentrated DMSO formulations containing 4 mol dm^{-3} Li[NO$_3$]/Li[FSI].[34] The [FSI]$^-$ anion has also been demonstrated previously to contribute to improved performance and the formation of stable and reliable SEI at Li-metal interfaces,[35] particularly in HCEs,[10a,c] but, as discussed in the introductory section, is considered incompatible toward superoxide generation at the cathode of Li–O$_2$ cells.[12] While the measured efficiency of this process remains insufficient for any practical consideration (wherein values exceeding 99.97% would be required),[32] the stability enhancement achieved through formulation design is considerable for a DMSO-based system for Li–O$_2$ application and presently the largest stability demonstrated for an additive-free DMSO electrolyte. In the absence of strong SEI forming components between DMSO, [Pyrr$_{14}$][TFSI], and Li[TFSI], these comparisons suggest the origins of stabilization lie in affecting the reactivity of DMSO in the electrolyte, as opposed to dramatically reducing the reactivity (or reducing power) of the interface. While some SEI or surface film formation is certainly expected in all non-aqueous electrolytes at Li^0, the Li-metal remained silvery-grey in appearance after Li|Cu cell disassembly of the high *CE* formulations, indicative of only a thin and less substantial surface layer present (see Figure S5, Supporting Information).

To further compare the formulation effects on plating Li, voltage profiles for the initial polarization step in Li|Cu cells are presented in Figure 2 (viii). All electrolytes exhibit an initial multi-step, pre-plating capacity (Q_{init}, Table 1) on the first polarization of the Cu working electrode with an onset potential around 1.4–1.2 V versus Li$^+$/Li. This is related to any reactions with native oxides,[36] and to the beginning of electrolyte reductive decomposition that contributes to SEI formation. All Cu working electrodes were prepared by the same acid etch/wash procedure and, thus, major variations are ascribed to differences from the electrolytes. With the exception of $0.15x_{Li}$ in C(8:2), the trend in reducing Q_{init} corresponds to the trend in increasing the resulting average Columbic efficiencies. The optimized formulations appear to be more resistant to reductive decomposition reactions, while the more dilute formulations undergo increased decomposition at low potentials, accounting somewhat for the loss of efficiency in subsequent cycling. Nevertheless, the optimized formulations, wherein the introduction of the IL to concentrated electrolytes improves cycling efficiencies, also undergo pre-plating processes that may contribute to an improved SEI layer.

Towards further understanding any stabilization effects arising from the high Li concentrations and/or IL component, the surfaces of Li metal were studied by X-ray photoelectron spectroscopy (XPS) after various treatments in select formulations (x_{Li} = 0.1 in A(1:0); 0.2 in A(1:0); 0.2 in C(8:2), see Figure S6, Supporting Information). When left to soak in the electrolytes for a week, the more dilute (least stable) formulation presented evidence of more substantial quantities of carbonate-type

decomposition products in O 1s, C 1s, and Li 1s spectra, while the more concentrated binary and ternary formulations showed similar features combined with evidence of further inorganic phases (including LiF, $-NSO_2CF_3$, and Li_3N) arising from preferential breakdown of the, more abundant, anion components. However, all three formulations exhibited a strong metallic Li^0 peak after soaking. When the Li was instead galvanostatically cycled within the more concentrated formulations (in Li|Li cells through 100 cycles), metallic Li^0 was no longer observed, indicating the growth of a more substantial surface layer. Comparing both the concentrated electrolytes, $x_{Li} = 0.2$ in A(1:0) and 0.2 in C(8:2), broadly similar features in the XPS are presented when undergoing the same treatment (i.e., soaking or cycling). However, notably the Li surface cycled in the IL-free binary formulation contains more pronounced evidence for $-NSO_2CF_3$ and SO_2/SO_3 species in the S 2p spectra (and complementary CF_x/LiF species) arising from anion reactions, despite the bulk ternary electrolyte containing a larger overall molar fraction of the $[TFSI]^-$ anion. Since the IL and Li-salt share the same anion, it is difficult herein to differentiate the source of these components in the ternary mixture, but the SEI formation/evolution appears to be affected by stabilizing solvent interactions that modulate reductive decomposition reactions rather than abundance of reactive components. At $x_{DMSO}:x_{Li+} = 3.2:1$ in this ternary formulation, involvement of $[TFSI]^-$ within the first solvation sphere is expected and affects the DMSO-Li^+ interaction strength (discussed later) and, thus, appears to modify the mechanism of SEI evolution on cycling. Additionally, the ternary formulation (in cycled and soaked electrodes) produces only minor evidence of a small peak for the breakdown products of the $[Pyrr_{14}]^+$ cation contained within the noise in the N 1s spectra. Critically however, this N^+ feature observed here is much less pronounced than has been reported previously for the same IL in ether solvent blends,[37] and in the absence of molecular solvents,[38] both containing lower concentrations of the same Li[TFSI] salt. These subtle differences in our surface measurements may indicate the IL component in optimized ternary formulation could contribute to the formation of an improved SEI. Further studies, more focused on the surface and depth characterization under different testing regimes, are required to provide deeper insight into the nature of the SEI in these ternary formulations.
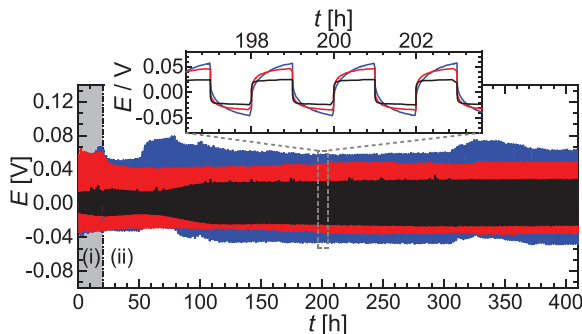
To represent the Li interface more closely to the environment of a Li–O_2 cell, wherein crossover of dissolved O_2 to the Li-metal anode is inevitable in the absence of any gas impermeable membrane, Li|Li cells were cycled under an O_2 atmosphere in several stable formulations where $x_{DMSO}/x_{Li} \leq 4$ (**Figure 3**). Following 10 plating/stripping cycles under Ar, cell enclosures were then filled with O_2 for the remaining cycles. Due to the nature of cell configuration and electrolyte filling, only dissolved O_2 would access Li-metal/electrolyte interfaces during cycling (i.e., Li-metal electrodes were not exposed to O_2 via a solid–gas interface). Therein, minimal changes in plating/stripping η were observed for successive cycles in all three studied electrolyte formulations. For comparison of the relative changes in η without transport property effects, the normalized voltage profiles are provided in Figure S7, Supporting Information. The IL-free electrolyte ($x_{Li} = 0.2$ in A(1:0)) displayed the largest increase relative to the first cycle overpotentials, but these deviations plateaued after 100 h. Some asymmetrical oscillations in the plating/stripping voltages can be seen in Figure 3 and these likely originate from the asymmetrical configuration of the ring versus disc electrodes of the Li|Li cell used for O_2 exposure (see Experimental Section, Supporting Information for details). Roberts et al. demonstrated that dissolved O_2 can improve the stability of Li^0-DMSO interfaces (in more dilute Li[ClO_4]-DMSO electrolytes).[15] However, XPS characterization of Li metal exposed to O_2 dissolved in a concentrated ternary formulation, $x_{Li} = 0.2$ in B(9:1), revealed no differences in the resulting surface layer compared to that soaked in Ar-saturated electrolyte (see Figure S6, Supporting Information). Therein, the Li was soaked in the formulation under Ar for 3 days prior to O_2 exposure. The effect of crossover of dissolved O_2 could have more pronounced effects on the interphase characteristics of an actively cycling electrode (due to possible exposure to fresh Li surfaces on dendrites or via fractures in the SEI during plating/stripping), but Figure 3 indicates this is minimal in the studied formulations and testing regime.

2.2. Li–O_2 Cell Performance

To further assess effects of formulation design, the electrochemical performance of the ternary formulations was explored in full Li–O_2 cells using simple carbon black/PTFE composite air electrodes without inclusion of any redox mediator or catalytic additive. As such, while optimization of cathode structure and facilitating oxidation of generated Li_2O_2 on charging remain critical challenges for Li–O_2 battery chemistry, these factors remain beyond the scope of the current study. Li–O_2 cells were cycled within a capacity limited regime to 500 mAh g^{-1} (with a 2–4.5 V vs Li^+/Li voltage range) and the (dis)charge voltage profiles and discharge capacities are shown in **Figure 4**. All electrolytes exhibit initial discharge plateaus around 2.7–2.8 V versus Li^+/Li associated with O_2 reduction and the generation of Li_2O_2 (see below). Slightly larger 1st cycle discharge overpotentials ($\approx$50–100 mV, with respect to 2.96 V vs Li^+/Li as the thermodynamic potential for Li_2O_2 formation) were observed in the IL + Li[TFSI] rich E formulations, and can be ascribed in part to poorer transport properties. On charging, however, the trends appear less straightforward with the presence of multiple
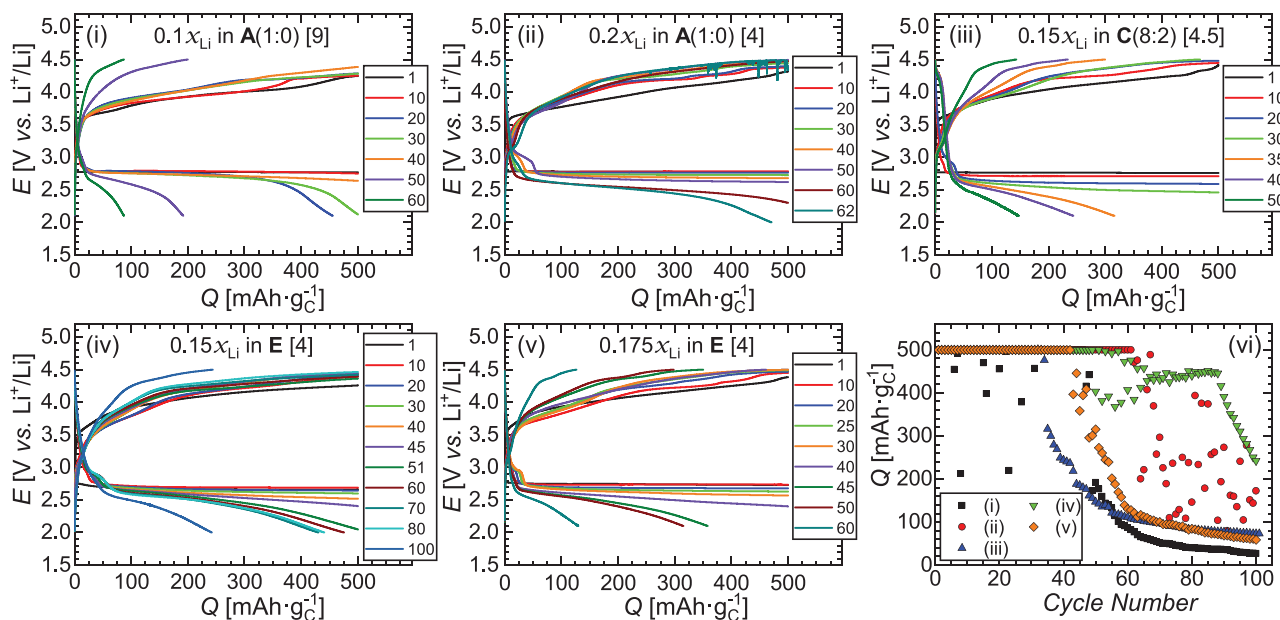

Figure 3. Voltage profiles of Li|Li cells cycled under O_2 atmosphere for $x_{Li} = 0.2$ in A(1:0) (black trace), $x_{Li} = 0.2$ in B(9:1) (red trace), and $x_{Li} = 0.15$ in E (blue trace). Cells were cycled at $j = \pm0.05$ mA cm^{-2} for 10 cycles under Ar (region (i)), then exposed to dry O_2 for the remaining cycles (region (ii)). Areal current density with respect to area of Li-ring electrode.

**ADVANCED
SCIENCE NEWS**

www.advancedsciencenews.com

**ADVANCED
FUNCTIONAL
MATERIALS**

www.afm-journal.de

Figure 4. Select voltage profiles of capacity limited (500 mAh g_C^{-1}) Li–O$_2$ cells cycled at $j = \pm60$ mA g^{-1} within a 2–4.5 V versus Li$^+$/Li voltage range. i) $0.1x_{Li}$ in A(1:0), ii) $0.2x_{Li}$ in A(1:0), iii) $0.15x_{Li}$ in C(8:2), iv) $0.15x_{Li}$ in E, v) $0.175x_{Li}$ in E, and vi) discharge capacity as a function of cycle number for cells (i–v). All capacities are calculated with respect to the mass of carbon black active material and legends in (i–iii) correspond to the cycle number.

sloped plateaus owing to the more complex processes of inevitable side reactions that may couple with Li$_2$O$_2$ oxidation.

It has been demonstrated previously that the solubility of intermediate LiO$_2$ (as well as the tendency for parasitic reactions on discharge) is suppressed by formulation of highly concentrated Li[TFSI]/DMSO solutions, where all DMSO molecules are considered to be "bound" dynamically in Li$^+$ cation solvation spheres.[16b] The stability of solvating DMSO, compared to that of "free" DMSO in solution, has also been computed to be improved with respect to attack by the generated superoxide radical.[16a] As will be explored later in this work, the characterization of free versus bound DMSO remains consistent in the ternary formulations, even with large IL proportions. This relationship, found to be critical to the electrochemical performance to that observed in Li|Li and Li|Cu cells, is persistent in the Li–O$_2$ cell performance. The discharge capacity delivered by the more dilute binary DMSO/Li[TFSI] mixture ($0.1x_{Li}$ in A(1:0)) began failing after 6 cycles (i.e., hitting the 2 V vs Li$^+$/Li discharge limit before delivering 500 mAh g^{-1}) This behavior was reproduced in this electrolyte and is associated with more rapid accumulation of passivating decomposition products at the interfaces, and the cycling proceeded erratically thereafter. The formulation $0.15x_{Li}$ in C(8:2) represents intermediate introduction of the IL component, yielding a reasonable improvement in cyclability wherein cell failure began after 34 cycles. In the more concentrated solutions, wherein x_{DMSO}:x_{Li} is fixed at 4:1, cycle lifetime of the Li–O$_2$ cells was increased further. The more concentrated binary mixture, $0.2x_{Li}$ in A(1:0), achieved target capacity for up to 60 cycles, at which point large sharp voltage oscillations occurred on charging and became more severe with cycling (see Figure 4 (ii), cycle 62 for the initial example). The ternary formulations $0.15x_{Li}$ and $0.175x_{Li}$ in E facilitated stable cycling up to 51 and 42 cycles, respectively, wherein growth in overpotentials is likely more exacerbated

due to the inherently more sluggish transport properties. To demonstrate the capability of these formulations to deliver high capacities, comparative Li–O$_2$ cells were cycled under a 1000 mAh g$_C^{-1}$ capacity limited-regime within the same voltage windows (Figure S8 (i–iv), Supporting Information). Therein, the more dilute formulation failed within 4 cycles while the concentrated binary and the optimized ternary formulations were able to deliver the full capacity for more than double this number of cycles to 9 and 12 cycles, respectively. Within the IL-free samples, charging capacity did not cease after cell failure and large plateaus associated with electrolyte decomposition above ≈4.3 V remain persistent. For the optimized ternary formulations, overpotentials grow steadily with cycling which suggests additional strategies to promote efficient recharge of the Li$_2$O$_2$, including utilization of enhanced cathode substrates and consideration of redox mediators, would be needed to enhance cycling lifetime. Within additional cells, both the optimized ternary formulation and the concentrated binary formulation were also capable of delivering over 5000 mAh g$_C^{-1}$ and 6000 mAh g$_C^{-1}$, respectively, in a single discharge (Figure S8 (v), Supporting Information).

2.3. Spectroscopy, Diffusion, and Simulation of Electrolyte Solvation Environments

The performance trends of these formulations in simplified Li–O$_2$ full cell configurations is inevitably complicated by more complex electrochemistry and side reactions occurring at the cathode (in addition to the challenges of Li plating/stripping and issues relating to poor transport properties). Utilizing ex situ Raman microscopy and X-ray diffraction, lithium peroxide (Li$_2$O$_2$) was identified as the primary discharge product in selected electrolytes (see Figures S9–S11 and further discussion in the Supporting Information).
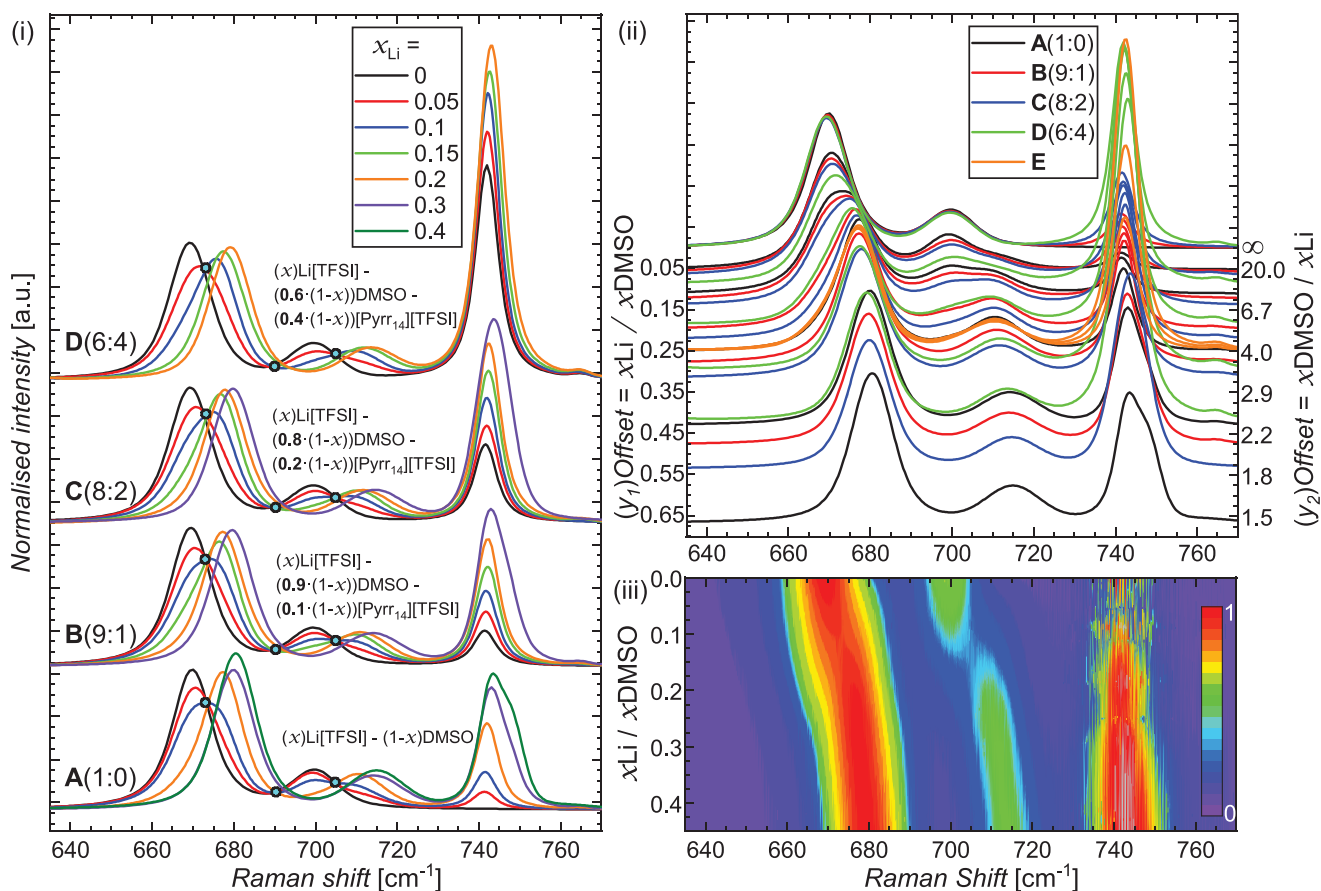
Figure 5. Raman spectra for ternary Li[TFSI]:DMSO:IL formulations. i) Spectra grouped by $x_{DMSO}:x_{[Pyrr14][TFSI]}$ ratios, ii) spectra stack plotted, and iii) intensity heat maps of all spectra, wherein the y-axis offset is proportional to the critical ratios between DMSO and Li[TFSI]. The color map in (iii) is scaled with respect to the intensity of $\delta_s(C-S)$ in pure DMSO. Isosbestic points in more dilute formulations (where free DMSO is observed) are shown by the blue circles at 673, 689, and 705 cm^{-1}.

Therein, simple carbon paper was used for the Li–O$_2$ cathodes and the same ex situ characterization methods supported that Li$_2$O$_2$ was removed upon recharging. Comprehensive characterization of changing Li$_2$O$_2$ formation/decomposition mechanisms are beyond the scope of the current investigation, but it is clear that a form of charging redox mediator or catalyst would be required herein to improve round-trip efficiency and avoid high voltage (>3.8 V) decomposition of electrolyte components and carbon electrode.[39] However, the initial observations persist; that higher fractions of Li-salt/IL in these mixtures yields improved stability and performance of the DMSO-based electrolyte, where the 4:1 ratio of DMSO:Li$^+$ remains critical even with the addition of IL. Raman spectroscopy was employed to investigate the solvation environments in the mixtures as a function of the ternary formulation. Therein, shifts in the symmetric and asymmetric C−S stretching modes of DMSO ($\delta_s(C-S)$ 669 cm^{-1} and $\delta_{as}(C-S)$ 699–700 cm^{-1}, respectively) have previously been used to explore interaction of DMSO with Li$^+$,[16b,40] and Na$^+$ cations.[41] Fortunately, these peaks do not overlap with any vibrational modes of [Pyrr$_{14}$]$^+$ or [TFSI]$^-$ components, facilitating this analysis across a wide ternary formulation range. These spectra across the range of 635–770 cm^{-1}, normalized with respect to DMSO content, are presented in

Figure 5 plotted by solution group (A–D, (i)) and stacked as a function of the critical $x_{DMSO}:x_{Li+}$ ratios (ii,iii).

Upon dissolution of Li[TFSI] salt in pure DMSO (A(1:0)), in addition to growth of a [TFSI]$^-$ peak ($\nu_s(S-N)$ and $\delta(CF_3)$) at ≈742 cm^{-1}, both DMSO modes shift to higher wavenumbers associated with Li$^+$-cation solvation and can each be deconvoluted into two overlapping peaks. For simplicity, the lower and higher wavenumber modes are described as free and bound DMSO, respectively, in solution. Further increasing the Li[TFSI] salt concentration leads to growth of a shoulder at ≈748 cm^{-1} (also labeled as bound for discussion) associated with aggregation or contact-ion pair (CIP) formation between [TFSI]$^-$ anion and partially solvated [Li-DMSO$_x$]$^+$ species. The same shift trends are further observed within the ternary formulations (B–D, Figure 5 (i)), although stronger shifts of the DMSO peaks to higher wavenumbers are observed for the IL-rich solutions of the same mole fraction of Li[TFSI]. To explore this, the binary DMSO/IL mixtures (in the absence of Li[TFSI]) are compared. Therein, no such shifts in the DMSO bands are observed as a function of IL content in the binary mixtures (Figure S12 (i), Supporting Information), indicating the absence of analogous DMSO-[Pyrr$_{14}$]$^+$ solvation interactions. Owing to the known complexity of the broad S=O stretching mode of

ADVANCED
SCIENCE NEWS
www.advancedsciencenews.com

ADVANCED
FUNCTIONAL
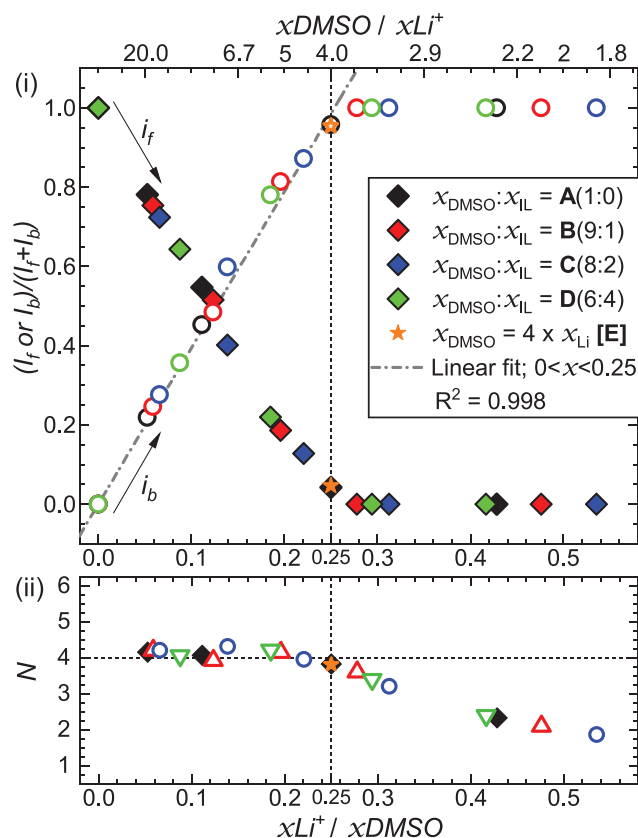**MATERIALS**
www.afm-journal.de

Figure 6. i) Proportion of free (closed shapes) and bound (open shapes) DMSO derived from integral intensities of fitted peaks for $\delta_{as}(C-S)$ and ii) coordination numbers, N, of DMSO in solvation sphere of the Li$^+$ cation (calculated using Equation 2) as a function of the x_{Li+}/x_{DMSO} ratios in the ternary formulations. Colors in (ii) correspond to solution groups in the legend of (i), and dashed guidelines highlight the critical 4:1 ratio. The orange star symbols show near-perfect overlap of three data points for solutions E.

DMSO (centered at ≈ 1040 cm^{-1}),[40a,42] and the overlapping of IL signals here, no such information on potential interactions can be straightforwardly obtained from this region (Figure S12 (ii), Supporting Information). However, consistent blue shifts in the weaker $-CH_3$ symmetric stretching mode of DMSO (2913 cm^{-1}) are observed in these binary mixtures with increasing IL content (Figure S12 (iii), Supporting Information). This is also observed in the DMSO/Li[TFSI] binary mixtures (Figure S13, Supporting Information) and may be attributed to anion solvation interactions and the disruption of self-association interactions of DMSO species in solution.[40a,42,43] Consequently, these observations indicate limited stabilizing interactions directly from the added IL component and, furthermore, reinforce the significance of the $x_{DMSO}:x_{Li+}$ ratios in the ternary formulation. This is further demonstrated when the spectra data are presented stacked as a function of $x_{DMSO}:x_{Li+}$ ratios (Figure 5 (ii,iii)), showing clear trends in the DMSO band shifting independently from the IL-content in a given formulation.

From the linear relationship between the [TFSI]$^-$ peak integral intensity and the $x_{[TFSI]-}/x_{DMSO}$ ratio in binary DMSO/Li[TFSI] mixtures, Tatara et al. affirm that the scattering coefficients of free and bound DMSO are comparable.[16b] This

linear relationship is observed here and is consistent across the entire studied ternary range (see Figure S14, Supporting Information). Peak fitting across the 635–770 cm^{-1} spectral range allows the derivation of the relative integral intensities for free (i_f) and bound (i_b) DMSO and [TFSI]$^-$ species and examples of the derived peak fitting are provided in Figure S15, Supporting Information. Utilizing Equation 2, based on the assumption of equal and consistent scattering coefficients for i_f and i_b, an estimation of coordination number (N) in [Li(DMSO)$_N$]$^+$ was derived using the asymmetric C—S stretching peaks at 699–715 cm^{-1}.

$$\frac{i_b}{i_f + i_b} = N \frac{x_{Li}[TFSI]}{x_{DMSO}} \tag{2}$$

The proportion of bound DMSO increases linearly with respect to the x_{Li+}/x_{DMSO} ratio in binary and ternary formulations up to $x_{Li+}/x_{DMSO} = 0.25$, independently of the amount of IL present in solution as presented in **Figure 6** (i). Therein, the derived coordination numbers in this formulation range ($N = \approx 4$, Figure 6 (ii) implies the prevalence for the formation of [Li(DMSO)$_4$]$^+$ complexes in solution. This is further supported by the slope of 3.94 for the linear fitting of the data from $0 < x_{Li+}/x_{DMSO} < 0.25$. At higher Li-salt concentrations where $x_{Li+}/x_{DMSO} > 0.25$ (or where the $x_{DMSO}:x_{Li+}$ ratio is less than the critical 4:1), no free DMSO was observed from the spectra of binary and ternary formulations. As such, $i_b / (i_f + i_b) = 1$ and derived N values become purely mathematical assumptions from prepared ratios between the two components. At this point, there are insufficient DMSO molecules in solution to form [Li(DMSO)$_4$]$^+$ complexes and the system will undergo formation of CIPs (e.g., [TFSI]$^-$–[Li(DMSO)$_x$]$^+$) and aggregate species wherein the more weakly donating [TFSI]$^-$ anion increases involvement in the first solvation spheres of Li$^+$ cations. This is also inferred from the growth of a higher wavenumber shoulder at ≈ 748 cm^{-1} (most prominent in IL-poor formulations) attributed to association of the [TFSI]$^-$ anion. Furthermore, in all formulation groups A–D, when $x_{DMSO}:x_{Li+} < 4:1$ the spectra deviates away from isosbestic points highlighted in less concentrated mixtures (blue circles in Figure 6 (i)). This is coupled with increasing shifts to higher wavenumbers of the bound DMSO peak, that otherwise remains mostly constant for all ternary formulations where $x_{DMSO}:x_{Li+} \geq 4:1$ (see Figure S16, Supporting Information in the SI). These observations further support deviations away from the prevalent [Li(DMSO)$_4$]$^+$ complex formation (through introduction of CIP or aggregate formation with [TFSI]$^-$ involvement and stronger DMSO–Li$^+$ interactions) in the highly concentrated formulations. The involvement of the [TFSI]$^-$ anion in CIPs/aggregates and the effects on the DMSO–Li$^+$ interaction strength may, consequently, affect the reactions contributing to the evolving SEI at cycling Li electrodes, as discussed earlier. A modified ternary plot highlighting the trends in free versus bound DMSO as a function of the three-component formulation is provided in Figure S17, Supporting Information.

The measured spectra and derived coordination numbers for DMSO/Li[TFSI] binary mixtures concurs with the work of Tatara et al.,[16b] and coordination numbers of ≈ 4 for other DMSO/Li-salt electrolytes have also been evaluated

elsewhere.[40b,c] Critically however, these trends remain persistent and unaffected even in the presence of relatively large quantities (up to 40 mol%) of [Pyrr$_{14}$][TFSI] IL. Additionally, while physical properties of the formulation change significantly with different IL contents (and could, in turn, be tuned/optimized), it is key that the relation of the critical 4:1 ratio to the electrochemical stability discussed earlier appears to relate almost exclusively to the nature of interactions between DMSO and Li$^+$, and is independent from interactions or interference

from the IL cation. To further investigate IL effects on solvation, spectra of the formulations labeled E where x_{DMSO}:$x_{Li[TFSI]}$ is fixed at 4:1 are presented in Figure S18, Supporting Information. Therein, in concentrated solutions where only the relative amount of IL is changing, the associated DMSO bands remain unaffected (as additionally indicated by the overlapping orange star symbols for the 3 different formulations in Figure 6). Interestingly, for all E formulations, the best fitting parameters result in residual lower frequency peaks for δ_s(C—S) and
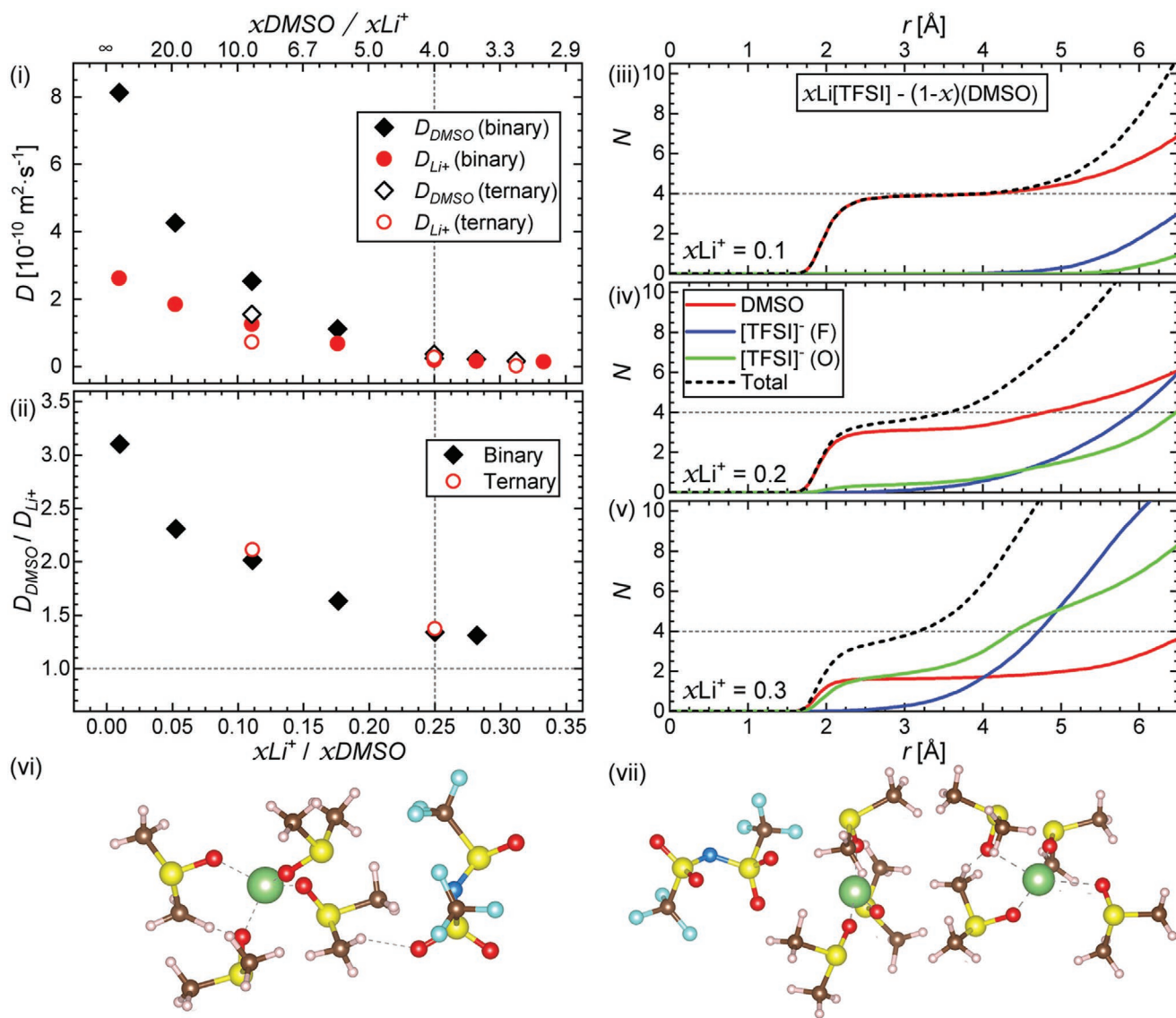

Figure 7. i) Diffusion coefficients (*D*) for DMSO (diamonds) and Li$^+$ (circles) in binary DMSO/Li[TFSI] (closed symbols) and ternary DMSO/[Pyrr$_{14}$][TFSI]/Li[TFSI] (open symbols) formulations as measured by PSGE-NMR at 298.15 K. ii) Ratio between D_{DMSO} and D_{Li+} from binary (diamonds) and ternary (circles) mixtures presented in (i). The molar fractions for DMSO/IL/Li-salt in the ternary mixtures used here at $x_{Li[TFSI]}/x_{DMSO}$ = 0.111 and 0.25 are 0.81/0.1/0.09 and 0.7/0.125/0.175, respectively and the numerical data for (i,ii) are provided in Table S2, Supporting Information. iii–v) Coordination numbers, *N*, of DMSO and [TFSI]$^-$ around Li$^+$ cations as a function of distance *r* derived from integration of AIMD-simulation RDFs for the DMSO/Li[TFSI] binary mixtures where $x_{Li[TFSI]}$ is 0.1 (iii), 0.2 (iv), and 0.3 (v). Panels (iv) and (v) represent average integrals for the 2 and 3 Li$^+$ cations, respectively, contained within the simulation box. Blue and green traces highlight respective distributions of O and F atoms of [TFSI]$^-$ molecules, highlighting preference for interactions via the S=O groups of the anion. vi,vii) AIMD-simulation snapshots of the solvation environments of Li$^+$ for the DMSO/Li[TFSI] binary mixtures where $x_{Li[TFSI]}$ is 0.1 (vi) and 0.2 (vii), corresponding to data shown in panels (iii,iv), respectively (brown = C, cyan = F, white = H, green = Li, blue = N, red = O, and yellow = S).

δ_{as}(C−S), indicating minor amounts of free DMSO (≈4.5%) present in these formulations. Overall, these collective observations indicate the IL cation behaves more as a spectator ion in solution rather than participating in any form of direct DMSO-IL stabilization interactions. While the strong electron donor DMSO molecule definitively interacts with, and solvates, dissolved Li$^+$ cations (both with and without IL), no evidence for the direct interaction with the softer, bulky, and sterically hindered [Pyrr$_{14}$]$^+$ cation (with and without Li$^+$ present) is found by Raman spectroscopy.

To further probe the nature of complex species in the binary and ternary formulations, the relative diffusional properties of DMSO and Li$^+$ was measured by pulsed-field gradient spin echo NMR (PGSE-NMR). Assuming strong DMSO–Li$^+$ association with long lifetimes, where PGSE-NMR enables measurement of averaged transport of nuclei from free and bound DMSO, the quotient of diffusion coefficients (D) of solvent and Li$^+$ cation should approach unity at (and beyond) the critical 4:1 ratio. The change in D of DMSO and Li$^+$, as well as their ratios (D_{DMSO}/D_{Li+}), as a function of formulation is shown in **Figure 7** (i,ii). The numerical data for PGSE-NMR measurements are provided in Table S2, Supporting Information. In agreement with the qualitative visual observation of reduced fluidity, D_{DMSO} and D_{Li+} both reduce as Li-salt concentrations are increased. Likewise, for the binary and ternary formulations where $x_{Li[TFSI]}/x_{DMSO}$ are equivalent, diffusion coefficients are lower for IL-containing ternary mixtures. However, even at and below the important 4:1 ratio of x_{DMSO} to x_{Li+}, D_{DMSO}, and D_{Li+} do not coalesce to the same value in either binary or ternary mixtures. This implies the presence of short-lived freely diffusing DMSO remaining in the highly concentrated formulations, despite no such free DMSO being observable (below 4:1) on the timescale of Raman spectroscopic measurements. Such ligand exchange dynamics could be further understood using time-resolved vibrational spectroscopy methods including 2D-infrared. Nevertheless, this observation and the derived diffusion coefficients are in good agreement with previous measurements on this binary DMSO/Li[TFSI] formulation (i.e., A[1:0]),[16b] and can be attributed to the shorter lifetime of stabilized [Li(DMSO)$_N$]$^+$ complexes relative to the timescale of NMR measurements (10^{-3} s). Crucially however, D_{DMSO}/D_{Li+} remains mostly unaffected by the addition of the IL, particularly where $x_{Li[TFSI]}/x_{DMSO}$ = 0.25 (wherein the vast majority of DMSO should be involved in Li$^+$ solvation according to the Raman characterization). This further alludes to the primarily spectator-like and non-competitive nature of the IL cation in this mixture with respect to DMSO interactions.

Ab initio molecular dynamics (AIMD) simulations of the local Li$^+$ environments in the binary formulations were performed at several concentrations in the A[1:0] DMSO/Li[TFSI] binary mixture. A simulation box containing 10 total molecules was constructed and, following simulation of the model systems (see the Supporting Information for computation details), radial distribution functions (RDFs) of DMSO (O) and [TFSI]$^-$ (O and F atoms) around the Li$^+$ cations were calculated, and the derived integral distributions are shown in Figure 7 (iii–v). Panels (iv,v) of Figure 7 represent the averaged distributions around the 2 and 3 Li$^+$ cations, respectively, in these simulations. Snapshots of the local solvation environment of Li$^+$ taken

from AIMD simulations for x_{Li+} = 0.1 and 0.2 are presented in Figure 7 (vi,viii), respectively. The snapshot for x_{Li+} = 0.3, corresponding to Figure 7 (v), is provided as Figure S19, Supporting Information.

In agreement with Raman measurements, where x_{Li+} = 0.1, the integral coordination number plateaus at $N \approx 4$ at 2–4 Å from the Li$^+$ center and this initial sphere is comprised entirely of DMSO (namely [Li(DMSO)$_4$]$^+$). Figure 7 (vi) shows the clear solvent separation of both cation and anion. In the more concentrated solutions, the solvation environment becomes more complex. Where x_{Li+} = 0.2 (Figure 7 (iv)), representing the 4:1 molar ratio, the derived coordination number plateaus just below 4 and residual levels of [TFSI]$^-$ (via the oxygen atoms of the anion) make up an important amount of the local Li$^+$ solvation environment in place of the less readily available DMSO. This is illustrated in Figure 7 (vii) where one Li$^+$ cation (right hand side) is completely coordinated by four DMSO molecules but the other (left hand side) experiences a partial solvation by DMSO, reducing the average value of N with competing interactions from the anion. This is in qualitative agreement with results of Raman and NMR diffusion experiments that indicated the presence of small quantities of free DMSO even at the 4:1 x_{DMSO}:x_{Li+} ratio. At higher concentrations still, three Li[TFSI] molecules are balanced out by only seven DMSO molecules and CIP/aggregate interactions make up for a significant proportion of the immediate surrounding layer of Li$^+$. Interestingly, as the concentration of Li[TFSI] increases, no obvious broad plateau of N is observed for the first sphere. Conversely, with sufficient DMSO molecules in the most dilute formulation (x_{Li+} = 0.1, Figure 7 (iii)), the beginning formation of the secondary sphere is quite distinct (i.e., at distances >4 Å), owing to significant solvent separation afforded between cation and anion.

3. Conclusions

The electrochemical stability of DMSO based electrolytes for Li–O$_2$ batteries was improved and optimized at Li-metal through wide-ranging formulation of ternary solvent/salt/IL mixtures. The introduction of a stable cyclic alkylammonium-[TFSI] IL and the tailoring of the important molar ratios between the three components resulted in significantly enhanced stability of Li-metal plating/stripping cycling, achieving >900 h cycling with no increase in overpotential. The Columbic efficiency of >94% of Li plating/stripping in optimized ternary mixtures, as measured in Li|Cu cells, was among the highest reported for DMSO-containing electrolytes, which remain highly relevant for Li–O$_2$ investigations and is significant since no strong SEI forming additives/components are utilized. Additionally, the introduction of dissolved O$_2$ gas has a limited effect on the instantaneous SEI formation in the ternary formulations and, subsequently, the Li cycling stability. Improved cycling performance in simplified Li–O$_2$ full cells was also demonstrated. Generally, from the electrochemical data, higher Li-salt and IL concentrations afforded improved electrolyte stabilities, analogous to HCEs. However, the specific importance of the DMSO/Li$^+$ molar ratio was apparent in the ternary electrolyte formulations and solutions were generally stable at a molar ratio of 4:1 (or less) for x_{DMSO}:x_{Li+}.

Through spectroscopic characterization, and complementary AIMD simulations, of the local solvation environment of DMSO and Li⁺, optimized molar ratios for enhanced DMSO stability were found to be related to the absence of free DMSO in solution. This relates to the stable first solvation spheres of DMSO to Li⁺ in solution and strong interactions with the high donor number DMSO, and correlates well with the electrochemical observations. While this has been observed in analogous binary mixtures previously, it critically holds true for the IL-containing ternary mixtures. Electrochemical stability deriving from the addition of the IL to already concentrated formulations (see Li|Cu and XPS) likely arises in-part from CIP/aggregate formation with excess anion species, and the effects strengthening Li⁺–DMSO bonding interaction, wherein DMSO is more deficient. These observations, combined with diffusional analysis of DMSO and Li⁺ and the lack of clear evidence for $[Pyrr_{14}]^+$ species in any SEI, indicate limited interactions (or effects) in the presence of the IL cation and suggests a spectator ion-like behavior. As such, while high concentrations of IL and Li-salt leads to viscosity and transport properties issues, the IL may be introduced here to modulate electrolyte properties, for example, vapor pressures (and contribute to anion/solvent interactions), without the cation significantly disturbing the key stabilizing complex formation involving DMSO and Li⁺. Therein, a comparison with the non-solvating diluents used in LHCEs may be drawn. Unlike ILs however, such LHCE diluents (fluorinated ethers) used, thus far, have been volatile species and would promote electrolyte evaporation under conventional Li–O₂ cell operation with a dynamic gas supply. Further optimization of transport properties and performances of the electrolytes reported here could consider the use of specifically tailored (lower viscosity) ILs/Li-salts, or even the possibility of quaternary solutions, carefully introducing non-solvating, thinning additives/diluents analogous to LHCE systems.

Supporting Information

Supporting Information is available from the Wiley Online Library or from the author.

Acknowledgements

Conflict of Interest

The authors declare no conflict of interest.

Data Availability Statement

The data that support the findings of this study are available from the corresponding author upon reasonable request.

[1] D. Aurbach, B. D. McCloskey, L. F. Nazar, P. G. Bruce, *Nat. Energy* **2016**, *1*, 16128.

[2] a) S. Wu, K. Zhu, J. Tang, K. Liao, S. Bai, J. Yi, Y. Yamauchi, M. Ishida, H. Zhou, *Energy Environ. Sci.* **2016**, *9*, 3262; b) J. Hassoun, H.-G. Jung, D.-J. Lee, J.-B. Park, K. Amine, Y.-K. Sun, B. Scrosati, *Nano Lett.* **2012**, *12*, 5775; c) H. Deng, F. Qiu, X. Li, H. Qin, S. Zhao, P. He, H. Zhou, *Electrochem. Commun.* **2017**, *78*, 11.

[3] X.-B. Cheng, C.-Z. Zhao, Y.-X. Yao, H. Liu, Q. Zhang, *Chem* **2019**, *5*, 74.

[4] H. T. T. Le, D. T. Ngo, P. N. Didwal, J. G. Fisher, C.-N. Park, I.-D. Kim, C.-J. Park, *J. Mater. Chem. A* **2019**, *7*, 3150.

[5] a) B. J. Bergner, M. R. Busche, R. Pinedo, B. B. Berkes, D. Schröder, J. Janek, *ACS Appl. Mater. Interfaces* **2016**, *8*, 7756; b) Y. Choi, K. Jung, H.-J. Kim, J.-W. Moon, J.-W. Lee, *Chem. Commun.* **2019**, *55*, 7643; c) W.-J. Kwak, H.-G. Jung, D. Aurbach, Y.-K. Sun, *Adv. Energy Mater.* **2017**, *7*, 1701232.

[6] M. Pasta, D. Armstrong, Z. L. Brown, J. Bu, M. R. Castell, P. Chen, A. Cocks, S. A. Corr, E. J. Cussen, E. Darnbrough, V. Deshpande, C. Doerrer, M. S. Dyer, H. El-Shinawi, N. Fleck, P. Grant, G. L. Gregory, C. Grovenor, L. J. Hardwick, J. T. S. Irvine, H. J. Lee, G. Li, E. Liberti, I. McClelland, C. Monroe, P. D. Nellist, P. R. Shearing, E. Shoko, W. Song, D. S. Jolly, C. I. Thomas, S. J. Turrell, M. Vestli, C. K. Williams, Y. Zhou, P. G. Bruce, *JPhysEnergy* **2020**, *2*, 032008.

[7] a) H. Ota, K. Shima, M. Ue, J.-i. Yamaki, *Electrochim. Acta* **2004**, *49*, 565; b) X.-Q. Zhang, X.-B. Cheng, X. Chen, C. Yan, Q. Zhang, *Adv. Funct. Mater.* **2017**, *27*, 1605989; c) V. Giordani, W. Walker, V. S. Bryantsev, J. Uddin, G. V. Chase, D. Addison, *J. Electrochem. Soc.* **2013**, *160*, A1544.

[8] a) F. Ding, W. Xu, G. L. Graff, J. Zhang, M. L. Sushko, X. Chen, Y. Shao, M. H. Engelhard, Z. Nie, J. Xiao, X. Liu, P. V. Sushko, J. Liu, J.-G. Zhang, *J. Am. Chem. Soc.* **2013**, *135*, 4450; b) W. Li, H. Yao, K. Yan, G. Zheng, Z. Liang, Y.-M. Chiang, Y. Cui, *Nat. Commun.* **2015**, *6*, 7436.

[9] a) W.-J. Kwak, S.-J. Park, H.-G. Jung, Y.-K. Sun, *Adv. Energy Mater.* **2018**, *8*, 1702258; b) Y. Yu, Y.-B. Yin, J.-L. Ma, Z.-W. Chang, T. Sun, Y.-H. Zhu, X.-Y. Yang, T. Liu, X.-B. Zhang, *Energy Storage Mater.* **2019**, *18*, 382; c) Y. Yu, X.-B. Zhang, *Matter* **2019**, *1*, 881; d) Y. Yu, G. Huang, J.-Z. Wang, K. Li, J.-L. Ma, X.-B. Zhang, *Adv. Mater.* **2020**, *32*, 2004157; e) B. Liu, W. Xu, J. Tao, P. Yan, J. Zheng, M. H. Engelhard, D. Lu, C. Wang, J.-G. Zhang, *Adv. Energy Mater.* **2018**, *8*, 1702340.

[10] a) J. Qian, W. A. Henderson, W. Xu, P. Bhattacharya, M. Engelhard, O. Borodin, J.-G. Zhang, *Nat. Commun.* **2015**, *6*, 6362; b) J. Zheng, J. A. Lochala, A. Kwok, Z. D. Deng, J. Xiao, *Adv. Sci.* **2017**, *4*, 1700032; c) X. Fan, L. Chen, X. Ji, T. Deng, S. Hou, J. Chen, J. Zheng, F. Wang, J. Jiang, K. Xu, C. Wang, *Chem* **2018**, *4*, 174; d) Q. Ma, Z. Fang, P. Liu, J. Ma, X. Qi, W. Feng, J. Nie, Y.-S. Hu, H. Li, X. Huang, L. Chen, Z. Zhou, *ChemElectroChem* **2016**, *3*, 531.

[11] S. A. Freunberger, Y. Chen, Z. Peng, J. M. Griffin, L. J. Hardwick, F. Bardé, P. Novák, P. G. Bruce, *J. Am. Chem. Soc.* **2011**, *133*, 8040.

[12] L. Grande, E. Paillard, G.-T. Kim, S. Monaco, S. Passerini, *Int. J. Mol. Sci.* **2014**, *15*, 8122.

[13] L. Johnson, C. Li, Z. Liu, Y. Chen, S. A. Freunberger, P. C. Ashok, B. B. Praveen, K. Dholakia, J.-M. Tarascon, P. G. Bruce, *Nat. Chem.* **2014**, *6*, 1091.

[14] D. G. Kwabi, T. P. Batcho, C. V. Amanchukwu, N. Ortiz-Vitoriano, P. Hammond, C. V. Thompson, Y. Shao-Horn, *J. Phys. Chem. Lett.* **2014**, *5*, 2850.

[15] M. Roberts, R. Younesi, W. Richardson, J. Liu, T. Gustafsson, J. Zhu, K. Edström, *ECS Electrochem. Lett.* **2014**, *3*, A62.

[16] a) B. Liu, W. Xu, P. Yan, S. T. Kim, M. H. Engelhard, X. Sun, D. Mei, J. Cho, C.-M. Wang, J.-G. Zhang, *Adv. Energy Mater.* **2017**, *7*, 1602605; b) R. Tatara, D. G. Kwabi, T. P. Batcho, M. Tulodziecki, K. Watanabe, H.-M. Kwon, M. L. Thomas, K. Ueno, C. V. Thompson, K. Dokko, Y. Shao-Horn, M. Watanabe, *J. Phys. Chem. C* **2017**, *121*, 9162; c) K. Pranay Reddy, P. Fischer, M. Marinaro, M. Wohlfahrt-Mehrens, *ChemElectroChem* **2018**, *5*, 2758.

[17] X. He, X. Liu, Q. Han, P. Zhang, X. Song, Y. Zhao, *Angew. Chem., Int. Ed.* **2020**, *59*, 6397.

[18] Y. Yu, G. Huang, J.-Y. Du, J.-Z. Wang, Y. Wang, Z.-J. Wu, X.-B. Zhang, *Energy Environ. Sci.* **2020**, *13*, 3075.

[19] a) G. A. Elia, J. Hassoun, W. J. Kwak, Y. K. Sun, B. Scrosati, F. Mueller, D. Bresser, S. Passerini, P. Oberhumer, N. Tsiouvaras, J. Reiter, *Nano Lett.* **2014**, *14*, 6572; b) J. Xie, Q. Dong, I. Madden, X. Yao, Q. Cheng, P. Dornath, W. Fan, D. Wang, *Nano Lett.* **2015**, *15*, 8371.

[20] J. Zhang, B. Sun, Y. Zhao, A. Tkacheva, Z. Liu, K. Yan, X. Guo, A. M. McDonagh, D. Shanmukaraj, C. Wang, T. Rojo, M. Armand, Z. Peng, G. Wang, *Nat. Commun.* **2019**, *10*, 602.

[21] a) C. Schütter, A. R. Neale, P. Wilde, P. Goodrich, C. Hardacre, S. Passerini, J. Jacquemin, A. Balducci, *Electrochim. Acta* **2016**, *220*, 146; b) A. R. Neale, P. Goodrich, T.-L. Hughes, C. Hardacre, S. C. Ball, J. Jacquemin, *J. Electrochem. Soc.* **2017**, *164*, H5124; c) K. Oldiges, D. Diddens, M. Ebrahiminia, J. B. Hooper, I. Cekic-Laskovic, A. Heuer, D. Bedrov, M. Winter, G. Brunklaus, *Phys. Chem. Chem. Phys.* **2018**, *20*, 16579; d) S. I. Wong, H. Lin, J. Sunarso, B. T. Wong, B. Jia, *Appl. Mater. Today* **2020**, *18*, 100522; e) G. H. Lane, A. S. Best, D. R. MacFarlane, M. Forsyth, P. M. Bayley, A. F. Hollenkamp, *Electrochim. Acta* **2010**, *55*, 8947.

[22] a) A. Khan, C. Zhao, *Electrochem. Commun.* **2014**, *49*, 1; b) A. Khan, C. Zhao, *ACS Sustain. Chem. Eng.* **2016**, *4*, 506.

[23] A. R. Neale, S. Murphy, P. Goodrich, C. Hardacre, J. Jacquemin, *ChemPhysChem* **2017**, *18*, 2040.

[24] A. R. Neale, P. Li, J. Jacquemin, P. Goodrich, S. C. Ball, R. G. Compton, C. Hardacre, *Phys. Chem. Chem. Phys.* **2016**, *18*, 11251.

[25] a) L. Grande, J. von Zamory, S. L. Koch, J. Kalhoff, E. Paillard, S. Passerini, *ACS Appl. Mater. Interfaces* **2015**, *7*, 5950; b) P. C. Howlett, D. R. MacFarlane, A. F. Hollenkamp, *Electrochem. Solid-State Lett.* **2004**, *7*, A97.

[26] A. L. Michan, B. S. Parimalam, M. Leskes, R. N. Kerber, T. Yoon, C. P. Grey, B. L. Lucht, *Chem. Mater.* **2016**, *28*, 8149.

[27] H. Xiang, P. Shi, P. Bhattacharya, X. Chen, D. Mei, M. E. Bowden, J. Zheng, J.-G. Zhang, W. Xu, *J. Power Sources* **2016**, *318*, 170.

[28] H. Sano, M. Kitta, H. Matsumoto, *J. Electrochem. Soc.* **2016**, *163*, D3076.

[29] a) L. Suo, Y.-S. Hu, H. Li, M. Armand, L. Chen, *Nat. Commun.* **2013**, *4*, 1481; b) J. Qian, W. A. Henderson, W. Xu, P. Bhattacharya, M. Engelhard, O. Borodin, J.-G. Zhang, *Nat. Commun.* **2015**, *6*, 6362; c) L. E. Camacho-Forero, T. W. Smith, P. B. Balbuena, *J. Phys. Chem. C* **2017**, *121*, 182.

[30] a) H. Zhang, W. Qu, N. Chen, Y. Huang, L. Li, F. Wu, R. Chen, *Electrochim. Acta* **2018**, *285*, 78; b) A. Basile, A. F. Hollenkamp, A. I. Bhatt, A. P. O'Mullane, *Electrochem. Commun.* **2013**, *27*, 69; c) A. Basile, A. I. Bhatt, A. P. O'Mullane, *Nat. Commun.* **2016**, *7*, 11794; d) N. Schweikert, A. Hofmann, M. Schulz, M. Scheuermann, S. T. Boles, T. Hanemann, H. Hahn, S. Indris, *J. Power Sources* **2013**, *228*, 237.

[31] N.-W. Li, Y.-X. Yin, J.-Y. Li, C.-H. Zhang, Y.-G. Guo, *Adv. Sci.* **2017**, *4*, 1600400.

[32] P. Albertus, S. Babinec, S. Litzelman, A. Newman, *Nat. Energy* **2018**, *3*, 16.

[33] B. D. Adams, J. Zheng, X. Ren, W. Xu, J. G. Zhang, *Adv. Energy Mater.* **2018**, *8*, 1702097.

[34] S. Eijima, H. Sonoki, M. Matsumoto, S. Taminato, D. Mori, N. Imanishi, *J. Electrochem. Soc.* **2019**, *166*, A5421.

[35] I. A. Shkrob, T. W. Marin, Y. Zhu, D. P. Abraham, *J. Phys. Chem. C* **2014**, *118*, 19661.

[36] a) H. Sano, H. Sakaebe, H. Senoh, H. Matsumoto, *J. Electrochem. Soc.* **2014**, *161*, A1236; b) Z. Zhang, X. Xu, S. Wang, Z. Peng, M. Liu, J. Zhou, C. Shen, D. Wang, *ACS Appl. Mater. Interfaces* **2016**, *8*, 26801.

[37] J. Zheng, M. Gu, H. Chen, P. Meduri, M. H. Engelhard, J.-G. Zhang, J. Liu, J. Xiao, *J. Mater. Chem. A* **2013**, *1*, 8464.

[38] P. C. Howlett, N. Brack, A. F. Hollenkamp, M. Forsyth, D. R. MacFarlane, *J. Electrochem. Soc.* **2006**, *153*, A595.

[39] M. M. Ottakam Thotiyl, S. A. Freunberger, Z. Peng, P. G. Bruce, *J. Am. Chem. Soc.* **2013**, *135*, 494.

[40] a) M. I. Gorobets, M. B. Ataev, M. M. Gafurov, S. A. Kirillov, *J. Mol. Liq.* **2015**, *205*, 98; b) X. Xuan, J. Wang, Y. Zhao, J. Zhu, *J. Raman Spectrosc.* **2007**, *38*, 865; c) Y. Yamada, Y. Takazawa, K. Miyazaki, T. Abe, *J. Phys. Chem. C* **2010**, *114*, 11680.

[41] M. He, K. C. Lau, X. Ren, N. Xiao, W. D. McCulloch, L. A. Curtiss, Y. Wu, *Angew. Chem., Int. Ed.* **2016**, *55*, 15310.

[42] K. Wakabayashi, Y. Maeda, K. Ozutsumi, H. Ohtaki, *J. Mol. Liq.* **2004**, *110*, 43.

[43] Z. Wang, B. Huang, S. Wang, R. Xue, X. Huang, L. Chen, *Electrochim. Acta* **1997**, *42*, 2611.